Journal of Alloys and Compounds 480 (2009) 834–838

Contents lists available at ScienceDirect

Journal of Alloys and Compounds

journal homepage: www.elsevier.com/locate/jallcom

Phase diagram and electrical conductivity of the AgBr–$NdBr_3$ binary system

P. Kolodziej[a], M. Szymanska-Kolodziej[a], I. Chojnacka[a], L. Rycerz[a], M. Gaune-Escard[b,*]

[a] Chemical Metallurgy Group, Faculty of Chemistry, Wroclaw University of Technology, Wybrzeze Wyspianskiego 27, 50-370 Wroclaw, Poland
[b] Ecole Polytechnique, IUSTI CNRS UMR 6595, Technopole de Chateau-Gombert, 5 rue Enrico Fermi, 13453 Marseille Cedex 13, France

ARTICLE INFO

Article history:
Received 24 November 2008
Received in revised form 10 February 2009
Accepted 14 February 2009
Available online 4 March 2009

Keywords:
Rare earth alloys and compounds
Thermodynamic properties
Thermochemistry
Thermal analysis
Phase diagram

ABSTRACT

DSC was used to investigate phase equilibrium in the AgBr–$NdBr_3$ system. This binary mixture was characterized as an eutectic system with solid solutions. The eutectic composition and temperature were found to be: x(AgBr) = 0.845 and T_{eut} = 647 K, respectively. In addition, the $AgNd_3Br_{10}$ compound was also evidenced; it decomposes in the solid state at 634 K.

The electrical conductivity of AgBr–$NdBr_3$ liquid mixtures, together with that of pure components, was measured down to temperatures below solidification. Results obtained are discussed in terms of possible complex formation.

1. Introduction

The high ionic conductivity of some solid silver halide phases makes them good candidates for a number of technological applications such as solid electrolytes in electrochemical power systems [1] or solid-state lasers that operate in the middle-infrared spectral range [2–8]. The luminescence of AgBr, AgCl, and $AgCl_xBr_{1-x}$ crystals and fibers doped with several lanthanide Ln^{3+} ions was investigated in the middle-infrared range [2–8]. These materials are highly transparent in the near and mid-IR ranges and have desirable mechanical and optical properties. They may therefore serve as suitable hosts for mid-IR solid-state lasers. Rare earth ions are characterized by complex energy level schemes, with some optical transitions of these ions being in the mid-IR range. Similar transitions or transitions between higher excited states may exist in silver halides. Incorporating rare earth in silver halide crystals and fibers may induce amplification and lasing in mid-IR.

The absorption, emission, and kinetic parameters were measured over a broad temperature range, evidencing strong luminescence in the spectral range 4–5.5 μm at room temperature. No noticeable differences were observed between the crystals and the fibers. Various optical parameters were calculated, which indicate in conjunction with experimental results that these doped crystals and fibers would be good candidates for the fabrication of mid-IR solid-state lasers or fiber lasers.

Therefore the knowledge of basic, thermodynamic and transport properties is of significant interest for these silver–lanthanide halide systems.

Following the thermodynamic and transport properties of the AgCl–$NdCl_3$ system [9] that we have investigated previously, the present work focused on the lanthanide–silver halide systems. It reports the phase diagram and the electrical conductivity of the AgBr–$NdBr_3$ liquid mixtures.

2. Experimental

2.1. Chemicals

Neodymium(III) bromide was synthesized from neodymium(III) oxide (Aldrich 99.9%). Nd_2O_3 was dissolved in hot concentrated HBr acid. The solution was evaporated and $NdBr_3 \cdot xH_2O$ was crystallized. Ammonium bromide was then added (20 mass%) and this wet mixture of hydrated $NdBr_3$ and NH_4Br was first slowly heated up to 450 and then up to 570 K to remove the water. The resulting mixture was subsequently heated to 670 K for sublimation of NH_4Br. Finally, the salt was melted at 1100 K under argon atmosphere. Crude $NdBr_3$ was purified by distillation under reduced pressure (~0.1 Pa) in a quartz ampoule at 1150 K. $NdBr_3$ prepared in this way was of high purity—min. 99.9%. Chemical analysis was performed by mercurimetric (bromine) and complexometric (neodymium) methods. The results were as follows: Nd, 37.55 ± 0.15% (37.57% theoretical), and Br, 62.45 ± 0.11% (62.43% theoretical).

Silver bromide was obtained by titration of silver nitrate (POCh Gliwice, p.a.) solution with KBr (Merck Suprapur, min. 99.9%) solution. The precipitate of AgBr was washed several times with deionized water in order to remove nitrate ions adsorbed on its surface. It was subsequently slowly heated under gaseous HBr atmosphere up to 650 K and cooled down to ambient temperature under argon atmosphere. AgBr prepared in this way was transferred into the glove-box and sealed-off in glass ampoules.

The appropriate amounts of $NdBr_3$ and AgBr were melted in vacuum-sealed quartz ampoules. The melts were homogenized and solidified. These samples were

* Corresponding author.
E-mail address: Molten.Salts@polytech.univ-mrs.fr (M. Gaune-Escard).

0925-8388/$ – see front matter © 2009 Elsevier B.V. All rights reserved.
doi:10.1016/j.jallcom.2009.02.083

Table 1
DSC results for AgBr–$NdBr_3$ binary system.

x_{AgBr}	T_{dec} (K) heating	T_{eut} (K) heating	T_{liq} (K) heating	T_{liq} (K) cooling
0.000	–	–	956	939
0.025	633	–	953	929
0.050	633	–	942	913
0.097	634	–	935	906
0.152	634	–	923	893
0.197	634	–	911	886
0.257	635	–	895	868
0.301	634	638	885	866
0.356	635	640	868	851
0.399	634	640	851	845
0.507	630	639	817	807
0.597	631	645	787	779
0.705	635	649	730	–
0.800	635	653	677	665
0.835	635	654	647	638
0.901	634	654	661	658
0.922	635	653	672	665
0.951	634	654	680	672
0.982	633	652	693	680
1.000	–	–	701	702

ground in an agate mortar in the glove-box. Homogenous mixtures of different compositions were prepared in this way and used in phase diagram measurements. The same procedure was used for the preparation of homogenous mixtures for electrical conductivity measurements.

All chemicals were handled inside a high purity argon atmosphere in the glove-box (water content <2 ppm). As silver bromide is sensitive to UV–vis light, all the manipulations were carried out under red light.

2.2. Measurements

A Setaram DSC 121 Differential Scanning Calorimeter was used to investigate phase equilibrium in the AgBr–$NdBr_3$ system. The calibration procedure (experimental temperature scale and enthalpy) of the DSC 121 was described previously [10,11]. Experimental samples (300–500 mg) were contained in vacuum-sealed quartz ampoules (about 6 mm diameter, 15 mm length) sealed under reduced pressure of argon. The sidewalls of ampoules were grounded in order to fit the cells snugly into the heat flow detector. Experiments were conducted at heating and cooling rates within the range 0.3–5 K min^{-1}.

Electrical conductivity measurements were carried out in a capillary quartz cell with cylindrical platinum electrodes, described in detail elsewhere [12]. Prior to experiment, each cell was calibrated at high temperature with pure molten NaCl [13]. The cell, filled with the substance under investigation, was placed into a stainless steel block, used to achieve a uniform temperature, inside a furnace. The conductivity of the melt was measured by platinum electrodes with the conductivity meter Tacussel CD 810 during increasing and decreasing temperature runs. The mean values of these two runs were used in calculations. Experimental runs were performed at heating and cooling rates 1 K min^{-1}. Temperature was measured with a Pt/Pt–Rh(10) thermocouple with 1 K accuracy. Temperature and conductivity data acquisition was made with PC computer, interfaced to the conductivity meter. All measurements were carried out under static argon atmosphere. The accuracy of the measurements was about ±2%.

3. Results and discussion

3.1. Phase diagram

DSC investigations were performed on samples with different compositions and yielded both the temperature and the fusion enthalpy of the concerned mixtures. Due to a noticeable supercooling effect during most cooling runs (Table 1), all experimental temperature and enthalpy data reported here were determined from heating curves.

The first series of measurements was performed at the heating rate 5 K min^{-1}. In the composition range $0 < x < 0.250$, where x is AgBr mole fraction, two endothermic peaks were present in all heating thermograms (Fig. 1A, $x = 0.1987$). The first effect, at 633 K, was first supposedly ascribed to the AgBr–$NdBr_3$ eutectic, whereas the second one to the liquidus temperature. However, DSC experiments performed on mixtures of composition $x > 0.250$ resulted

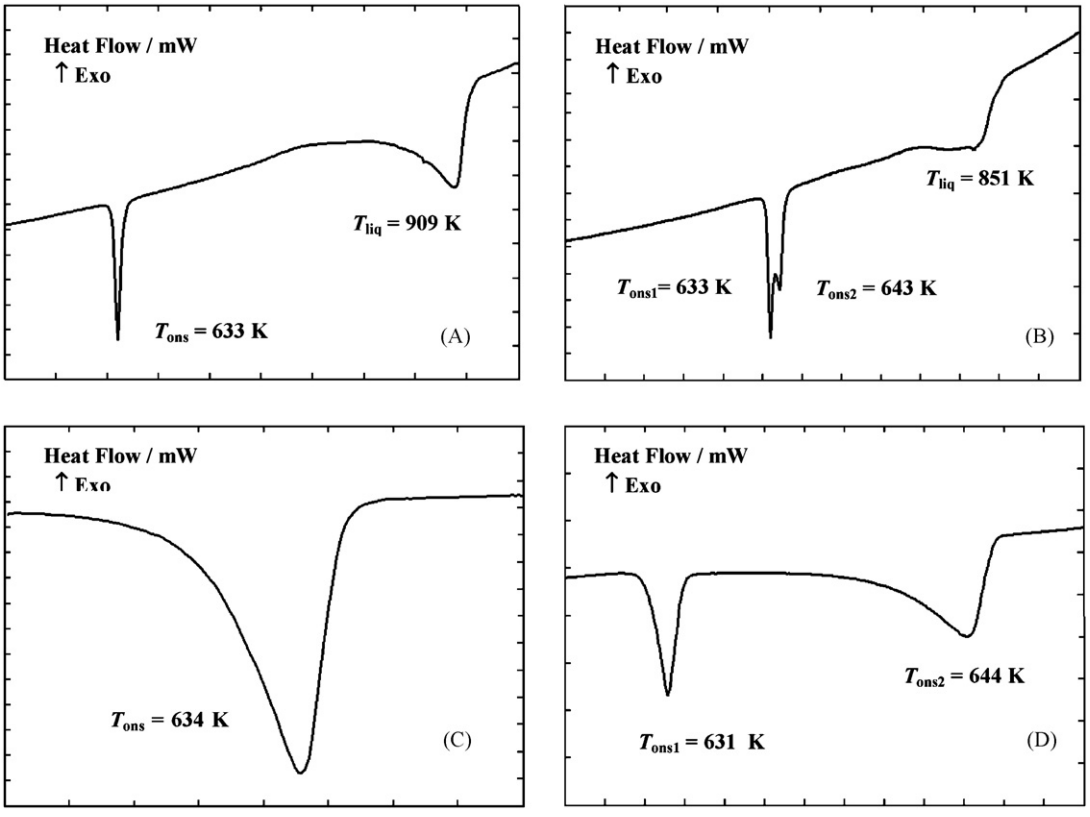

Fig. 1. DSC heating curves for AgBr–$NdBr_3$ mixtures of different compositions: (A) x, AgBr = 0.197, heating rate 5 K min^{-1}, (B) x, AgBr = 0.399, heating rate 5 K min^{-1}, (C) x, AgBr = 0.152, heating rate 0.3 K min^{-1}, (D) x, AgBr = 0.597, heating rate 0.3 K min^{-1}.

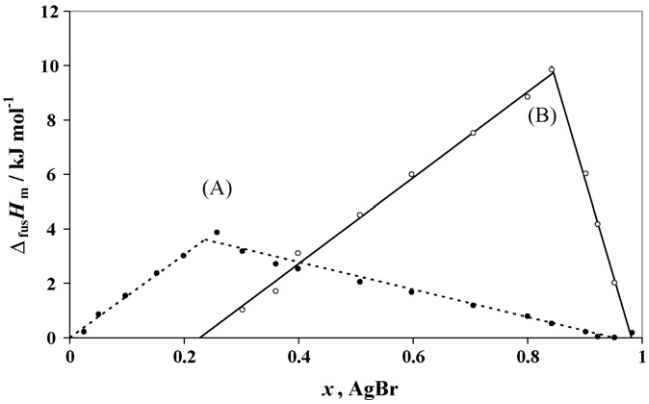

Fig. 2. Tamman construction for compound and eutectic determination in the AgBr–$NdBr_3$ system: (A) determination of compound composition and (B) determination of eutectic composition.

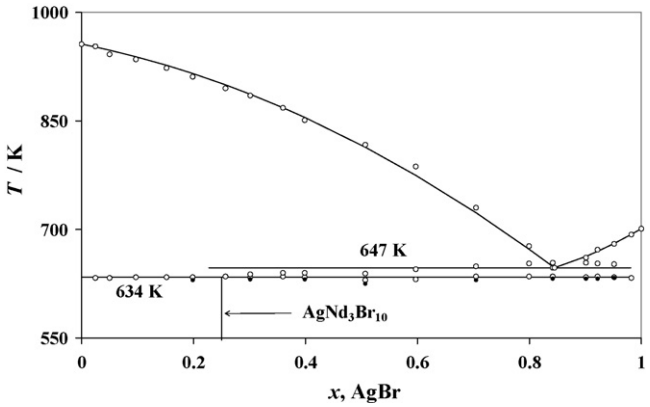

Fig. 3. Phase diagram of AgBr–$NdBr_3$ binary system.

in thermograms with two endothermic peaks followed by a third and final thermal event corresponding to the liquidus temperature (Fig. 1B). The first and second endothermic effects at about 633 and 643 K, respectively, overlapping each other, suggest that the system is not of the simple eutectic type. Measurements at low heating rate (0.3 K min^{-1}) were performed in order to resolve these two merged thermal events. It should be pointed out that the method used for calibrating the apparatus eliminates the influence of the heating rate on the measured temperature. These measurements generally confirmed the observations made at the heating rate 5 K min^{-1}, *i.e.* one endothermic effect for mixtures in the mole fraction range $x < 0.250$ (Fig. 1C) and two endothermic effects in samples corresponding to $x > 0.250$ (Fig. 1D) at the average temperatures 634 and 647 K, respectively. The first effect appeared for all range of composition, *i.e.* $0 < x < 1$ and can be attributed to the compound decomposition in the solid state. The composition of this compound was determined accurately from the so-called Tamman plot (Fig. 2A) of the experimental enthalpy related to this effect vs. composition. This plot suggests for the compound the stoichiometry $AgNd_3Br_{10}$ ($x_{theor} = 0.25$, $x_{found} = 0.236 \pm 0.020$). This compound decomposes in the solid state with an enthalpy of about 56.4 ± 0.5 kJ mol^{-1}. The second thermal event, at 647 K, existing in the mixtures with $x > 0.25$, could be undoubtedly ascribed to the AgBr–$NdBr_3$ eutectic effect. The eutectic contribution to the enthalpy of fusion was determined and plotted against composition in Fig. 2B. This Tamman construction made it possible to evaluate the eutectic composition accurately from the intercept of the two linear parts in Fig. 2B, as $x_E = 0.845 \pm 0.005$. The AgBr–$NdBr_3$ eutectic mixture melts with the enthalpy $\Delta_{fus}H_m = 9.7 \pm 0.4$ kJ mol^{-1}. This Tamman construction also gives information about the formation of solid solutions both in the $NdBr_3$- and AgBr-rich sides. Accordingly, the corresponding straight lines were not forced to intercept the composition axis at $x = 0$, and $x = 1$. The AgBr molar fraction ranges at which solid solutions may exist at 647 K were determined as $x \leq 0.227 \pm 0.013$, and $x \geq 0.981 \pm 0.005$, respectively (Fig. 2B).

It must be pointed out that in some samples an additional, small endothermic effect was observed at about 631 K in the composition range $x = 0.20$–0.95. The enthalpy related to this effect varied from 0.02 to 0.2 kJ mol^{-1}. However this effect could not be detected on the whole composition range indicated above. For example it appeared in the sample with AgBr molar fraction $x = 0.301$, disappeared completely in the sample with $x = 0.360$ and appeared once again in the sample with $x = 0.399$. It has been impossible to evidence any composition dependence for the enthalpy of this effect or to formulate any hypothesis as for its origin. The lack of this effect in some samples excludes however its origin from impurities in the starting compounds, since they would have been observed in all samples prepared from the same batch.

The complete phase diagram constructed on the base of DSC experiments is presented in Fig. 3. These effects, of unknown origin, are presented as black circles in this figure. Unfortunately, we were unable to determine solidus temperatures in the areas where solid solutions exist. Generally, the topology of our AgBr–$NdBr_3$ phase diagram is in agreement with Molodkin et al.'s [14]. These authors also reported one stoichiometric compound decomposing in the solid state and evidenced the formation of solid solutions on both sides of the phase diagram. However, some significant differences from our results are observed. They have concluded that $Ag_2Nd_3Br_{11}$ forms from reaction of end-member components, but with no real argument for that. On heating, the compound decomposed at 643 K to yield a mixture of α and β solid solutions. It is very likely that those problems in the determination of compound composition were caused by the high heating rates (10–15 K min^{-1}) employed.

As explained above, the low heating rate (0.3 K min^{-1}) used in the present work made it possible to identify with confidence the compound as $AgNd_3Br_{10}$. Also in contrast to Molodkin et al. [14], we found that this compound exists up to a $NdBr_3$ molar fraction close to 1. There are also small differences in the eutectic temperature 647 K and composition $x = 0.845$ (0.877 and 655 K, respectively [14]).

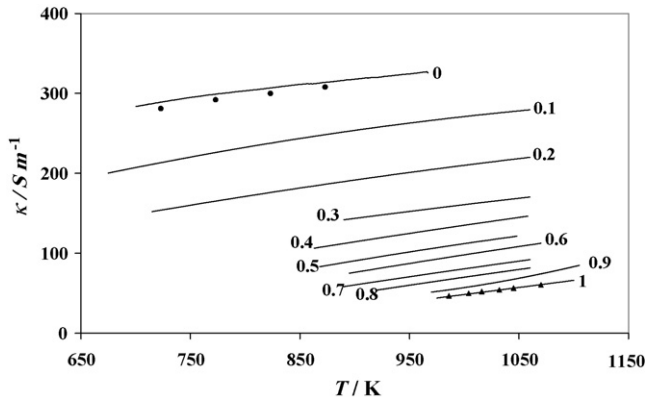

Fig. 4. Electrical conductivity of molten AgBr–$NdBr_3$ mixtures vs. temperature: numbers—molar fraction of $NdBr_3$, black circles—literature data on AgBr [17], black triangles—literature data on $NdBr_3$ [16].

Table 2
Coefficients in equation: $\kappa = A + BT + CT^2$ for AgBr–$NdBr_3$ liquid mixtures.

x, $NdBr_3$	A (S m^{-1})	B ($\times 10^1$ S m^{-1} K^{-1})	C ($\times 10^4$ S m^{-1} K^{-2})	Temperature range (K)
0.00	50.85	4.638	−1.856	710–1060
0.100	−81.02	5.511	−1.990	675–1060
0.200	−67.04	3.803	−1.030	715–1060
0.300	−78.11	3.132	−7.420	760–1060
0.400	−135.97	3.419	−7.099	865–1060
0.500	−227.96	4.789	−1.391	868–1050
0.600	−188.05	3.607	−7.398	895–1070
0.700	−177.05	3.211	−6.249	890–1060
0.800	−191.97	3.270	−6.510	915–1060
0.900	412.04	−9.161	5.6111	950–1100
1.00	−108.33	1.377	1.896	956–1100

3.2. Electrical conductivity

The variation of molten salt resistance R_{exp} with frequency f can be expressed by

$$R_{exp} = R_{inf} + \frac{C}{\sqrt{f}} \quad (1)$$

where R_{exp} and R_{inf} are the resistance measured at frequency f and polarization-free resistance at infinite frequency, respectively. C is a constant characteristic of the melt under investigation. It contains polarization resistance and electrolyte capacitance terms, which were found to be proportional to $f^{-1/2}$ [15]. Thus Eq. (1) was used in processing all resistance data obtained in this work. Electrical conductivity measurements were carried out at the frequency 4 kHz and R_{inf} was calculated from Eq. (1). The value of C, necessary in this calculation, was determined from the frequency dependence of resistance, which was obtained from measurements carried out on the frequency range from 60 Hz to 16 kHz.

Prior to the measurements of binary mixtures, the conductivity of pure components was determined. Our conductivity data on $NdBr_3$ agree quite well with Dworkin et al. [16] with a deviation not exceeding 1.4% over the entire temperature range. Those relative to AgBr are about 2% larger than those reported by Tuband and Lorenz [17] in the whole temperature range.

The electrical conductivity of AgBr–$NdBr_3$ liquid mixtures was measured for the first time over the entire composition range in steps of 10 mol%. A second order polynomial dependence of conductivity κ on temperature was fitted to all experimental results:

$$\kappa = A + BT + CT^2 \text{ (in S m}^{-1}\text{)} \quad (2)$$

The electrical conductivity dependence on temperature is shown in Fig. 4 for AgBr, $NdBr_3$ and AgBr–$NdBr_3$ mixtures. The coefficients A, B, and C in Eq. (2) are displayed in Table 2. In Fig. 5 the

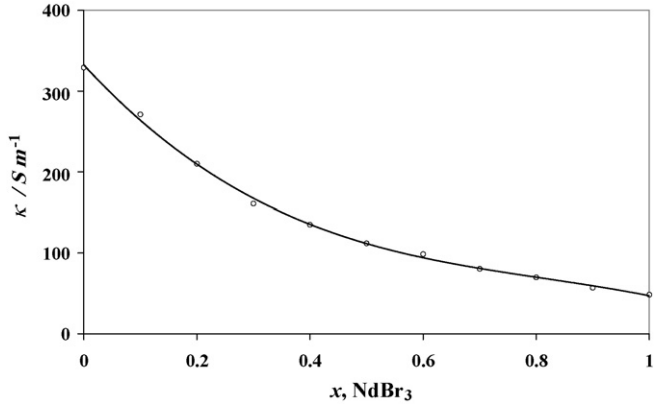

Fig. 5. Electrical conductivity isotherm of AgBr–$NdBr_3$ liquid mixtures at 1000 K.

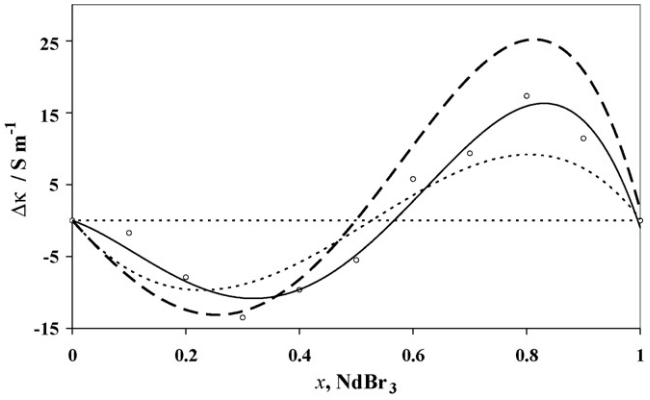

Fig. 6. Relative deviations of the electrical conductivity from the Kuroda equation (3) for AgBr–$NdBr_3$ liquid mixtures: open circles and solid line—AgBr–$NdBr_3$, thick broken line—AgCl–$NdCl_3$ [9], thin broken line—NaCl–$NdCl_3$.

conductivity isotherm at 1000 K was plotted against the mole fraction of $NdBr_3$. The specific conductivity decreases with increase of $NdBr_3$ concentration, with significantly larger changes in the silver bromide-rich region, as it should be expected. Decrease of AgBr molar fraction causes decrease of the mobile ions number (Ag^+, Br^-), which are carriers of electrical charge.

In many cases the composition dependence of specific conductivity of binary mixtures can be well represented by the Kuroda [18] equation:

$$\kappa = x_1^2\kappa_1 + x_2^2\kappa_2 + 2x_1x_2\kappa_1 \quad (3)$$

where x_1, x_2 are the mole fractions of the pure components, and κ_1, κ_2 are their specific conductivities, with $\kappa_1 < \kappa_2$. However, in the case of the liquid mixtures investigated here, significant deviations of experimental results from this equation were observed. These relative deviations, calculated from Eq. (4), are presented in Fig. 6.

$$\Delta\kappa = \frac{\kappa_{exp} - \kappa_{Kuroda}}{\kappa_{Kuroda}} \times 100\% \quad (4)$$

Negative deviations occur in the AgBr-rich composition range (minimum at about $x = 0.30$–0.35), and are followed by positive deviations starting from $x = 0.55$ (maximum around $x = 0.85$). The behavior of AgBr–$NdBr_3$ liquid mixtures is almost identical to that of AgCl–$NdCl_3$, both in the sense of negative and positive deviations and of their minimum and maximum location [9] (these data are also presented in Fig. 6). We also applied Eq. (4) to the conductivity data on NaCl–$NdCl_3$ liquid mixtures [19] because of the similarity of Ag^+ and Na^+ ionic radii (100 and 102 pm, respectively). The results of this calculation are also presented in Fig. 6.

According to literature [20,21], marked negative electrical conductivity deviations are strongly indicative of complex formation. If only one complex species exists in the melt, the absolute value of deviation reaches a maximum at the composition corresponding to the stoichiometry of this complex. If several complex species co-exist, the location of the minimum may slightly deviate from the exact stoichiometry of the predominant species. Therefore the existence of negative deviations in AgCl–$NdCl_3$ and AgBr–$NdBr_3$ liquid mixtures with a minimum $x \approx 0.25$ and $x \approx 0.30$–0.35, respectively, is indicative of $NdCl_6^{3-}$ and $NdBr_6^{3-}$ octahedral complexes formation in the melts. Unfortunately no experimental confirmation of their existence exists so far. However, taking into account the similarity of Ag^+ and Na^+ ionic radii, the results of different experimental techniques applied to the NaCl–$NdCl_3$ and NaBr–$NdBr_3$ liquid systems may bring further arguments about this hypothetical $NdCl_6^{3-}$ and $NdBr_6^{3-}$ complexes formation in the systems with silver chloride and silver bromide, respectively. Raman spectroscopic investigations [22] showed that octahedral LnX_6^{3-} ions are

formed in the MX–LnX_3 liquid mixtures (Ln = lanthanide, M = alkali metal, X = Cl, Br). These ions constitute the predominant species in the MX-rich liquid mixtures. As the LnX_3 concentration increases, distortion of octahedra, which are bridged by halide anions, takes place. Neodymium(III) complex formation in molten NaCl, KCl, RbCl, CsCl and $(Li–K)Cl_{eut}$ was evidenced by electronic spectroscopy [23]. Predominant octahedral local symmetry of Nd^{3+} was found over the entire composition range including pure molten $NdCl_3$. The formation of these LnX_6^{3-} complexes influences the electrical conductivity and induces the appearance of the negative deviation in the system NaCl–$NdCl_3$. The mixing enthalpy measurements performed on the MX–NdX_3 liquid mixtures [24,25] (X = Cl, Br) also suggested the existence of these octahedral complexes. This enthalpy, negative in all systems, was found to increase (in absolute value) with alkali metal cation size. Similarly, as described above for electrical conductivity deviations, the maximum mixing enthalpy (in absolute value) was situated at compositions of about 30–40 mol% NdX_3. This was ascribed to the possibility of NdX_6^{3-} complex formation. We had assumed that complex NdX_6^{3-} anions dominate in melts of neodymium(III) halide with alkali metal halides (especially for systems with heavier alkali metal cations), although the possibility of the existence of other forms of complex could not be excluded. These conclusions were confirmed by Raman spectroscopy investigations [22]. The octahedral NdX_6^{3-} complex ions were found to be the predominant species in MX-rich halide liquid mixtures. However, NdX_3 concentration increase leads to the distortion of these octahedra and to polymers formation (distorted octahedra which are bridged altogether by bromide anions).

Therefore, it is not unreasonable to assume that NdX_6^{3-} complexes also exist in the AgX–NdX_3 liquid mixtures. Accordingly, the minimum of negative electrical conductivity deviations from Eq. (3) is located at a NdX_3 molar fraction of about 0.25 and 0.30–0.35, for chloride and bromide system, respectively. The shift of the minimum in the latter system can be indicative of polymerized octahedral complexes as discussed above.

The positive deviations at NdX_3-rich compositions are apparently caused by the disruption of associates in pure NdX_3, resulting in a new structure in which neodymium halide (chloride or bromide) contributes more to the transfer of electricity.

The different magnitude of both negative and positive deviations in NaCl–$NdCl_3$ from one side and AgX–NdX_3 mixtures from the other is apparently caused by the different nature of Na^+ and Ag^+ ions. Na^+ (hard Lewis acid), with a noble gas configuration, has a spherical symmetry and low polarizability hard sphere. Its electronic cloud is rigid and prefers ionic bonding. On the other hand, Ag^+ with d^9 electron structure (soft Lewis acid) has a highly polarizable soft sphere. High quadrupolar polarizability (deformation from sphere into an ellipsoid) takes place in this ion [26]. Accordingly Na^+ is more halide attracting than Ag^+, or in other words, AgX is a better "donor" of halide ions than NaCl. Thus in AgX-rich melts the amount of NdX_6^{3-} complexes formed is larger than in NaCl-rich mixtures. Hence larger negative deviations of electrical conductivity in the AgX–NdX_3 system. In NdX_3-rich mixtures a disruption of polymeric structure takes place. It will be more marked in the case of a good halide ions donor (AgX) and result in a larger positive electrical conductivity deviations than in the NaCl–$NdCl_3$ melts.

4. Conclusion

The AgBr–$NdBr_3$ binary system is an eutectic system with solid solutions; it also includes the $AgNd_3Br_{10}$ compound, which decomposes in the solid state. These results were discussed critically with previous data from literature.

The specific electrical conductivity of AgBr–$NdBr_3$ liquid mixtures was also determined. It was discussed in terms of $NdBr_6^{3-}$ octahedral complexes formation in the melts.

Acknowledgements

Financial support by the Polish Ministry of Science and Higher Education from budget on science in 2007–2010 under the grant no. N204 4098 33 is gratefully acknowledged.

L.R. and I.Ch. wish to thank the Ecole Polytechnique de Marseille for hospitality and support during this work.

References

[1] C.S. Sunandana, P. Senthil Kumar, Bull. Mater. Sci. 27 (2004) 1.
[2] L. Nagli, A. German, A. Katzir, Opt. Mater. 16 (2001) 243.
[3] D. Bunimowich, L. Nagli, A. Katzir, Opt. Lett. 20 (1995) 2417.
[4] L. Nagli, D. Bunimovich, A. Schmilevich, N. Kristianpoller, A. Katzir, J. Appl. Phys. 74 (1993) 5737.
[5] L. Nagli, O. Gayer, A. Katzir, Opt. Lett. 30 (2005) 1831.
[6] L. Nagli, O. Gayer, A. Katzir, Opt. Mater. 28 (2006) 147.
[7] I. Szafir, O. Gayer, L. Nagli, S. Shalem, A. Katzir, J. Lumin. 126 (2007) 541.
[8] G. Brodetzki, O. Gayer, I. Sharif, L. Nagli, A. Katzir, J. Lumin. 128 (2008) 1323.
[9] M. Szymanska-Kolodziej, P. Kolodziej, L. Rycerz, M. Gaune-Escard, Z. Naturforsch. 63 (2008) 364.
[10] L. Rycerz, High Temperature Characterization of LnX_3 and LnX_3-AX Solid and Liquid Systems (Ln = Lanthanide, A = Alkali, X = Halide): Thermodynamics and Electrical Conductivity, Ph.D. Thesis, Marseille, 2003.
[11] L. Rycerz, Thermochemistry of lanthanide halides and compounds formed in lanthanide halide–alkali metal halide systems, (in Polish), Scientific Papers of Institute of Inorganic Chemistry and Metallurgy of Rare Elements, Wroclaw University of Technology, Series Monographs 35, Wroclaw, 2004.
[12] Y. Fouque, M. Gaune-Escard, W. Szczepaniak, A. Bogacz, J. Chim. Phys. 75 (1978) 360.
[13] G.I. Janz, J. Phys. Chem. Ref. Data 17 (Supplement no. 2) (1988).
[14] A.K. Molodkin, A.B. Strekachinskii, A.G. Dudareva, A.I. Ezhov, V.A. Krokin, Zh. Noerg. Khim. 26 (11) (1981) 3089.
[15] R.P.T. Tomkins, G.J. Janz, E. Andalaft, J. Electrochem. Soc. Electrochem. Sci. Technol. 117 (1970) 906.
[16] A.S. Dworkin, H.R. Bronstein, M.A. Bredig, J. Phys. Chem. 67 (1963) 2715.
[17] C. Tuband, E. Lorenz, Z. Phys. Chem., Abt. A 97 (1914) 513.
[18] J. Mochinaga, K. Cho, T. Kuroda, Denki Kagaku 36 (1968) 746.
[19] A. Potapov, L. Rycerz, M. Gaune-Escard, Z. Naturforsch. 62a (2007) 431.
[20] Yu.K. Delimarskii, B.F. Markov, Electrochemistry of Fused Salts, The Sigma Press Publishers, Washington, 1961.
[21] Yu.K. Delimarskii, Elektrokhimiia ionnyh rasplavov, Mietallurgiia, Moskva, 1978 (in Russian).
[22] G.M. Photiadis, B. Borresen, G.N. Papatheodorou, J. Chem. Soc. Faraday Trans. 17 (1998) 2605.
[23] Yu.A. Barbanel, Coordination Chemistry of f-Elements in Melts, Energoatomizdat, Moscow, 1985 (in Russian).
[24] M. Gaune-Escard, L. Rycerz, A. Bogacz, W. Szczepaniak, Thermochim. Acta 236 (1994) 67.
[25] M. Gaune-Escard, A. Bogacz, L. Rycerz, W. Szczepaniak, Thermochim. Acta 279 (1996) 11.
[26] L.M. Slifkin, Cryst. Latt. Def. Amorph. Mater. 18 (1989) 81.